Control of Superconductivity with a Single Ferromagnetic Layer in Niobium/Erbium Bilayers

N. Satchell,[1,2] J. D. S. Witt,[1] M. G. Flokstra,[3] S. L. Lee,[3] J. F. K. Cooper,[2] C. J. Kinane,[2] S. Langridge,[2] and G. Burnell[1,*]

[1]*School of Physics and Astronomy, University of Leeds, Leeds LS2 9JT, United Kingdom*

[2]*ISIS Neutron and Muon Source, STFC Rutherford Appleton Laboratory, Chilton, Didcot, Oxon OX11 0QX, United Kingdom*

[3]*School of Physics and Astronomy, SUPA, University of St Andrews, St Andrews KY16 9SS, United Kingdom*

(Received 27 January 2017; revised manuscript received 31 March 2017; published 28 April 2017)

Superconducting spintronics in hybrid superconductor-ferromagnet (*S*-*F*) heterostructures provides an exciting class of device. The prototypical superspintronic device is the superconducting spin valve, where the critical temperature T_c of the *S* layer can be controlled by the relative orientation of two (or more) *F* layers. Here, we show that such control is also possible in a simple *S*-*F* bilayer. Using field history to set the remanent magnetic state of a thin Er layer, we demonstrate for a Nb/Er bilayer a high level of control of both T_c and the shape of the resistive transition $R(T)$ to zero resistance. We are able to model the origin of the remanent magnetization, treating it as an increase in the effective exchange field of the ferromagnet and link the remanent magnetization using conventional *S*-*F* theory to the suppression of T_c. We observe stepped features in the $R(T)$, which we argue is due to a fundamental interaction of superconductivity with inhomogeneous ferromagnetism, a phenomena currently lacking theoretical description.

DOI: 10.1103/PhysRevApplied.7.044031

I. INTRODUCTION

While traditionally considered competing phenomena, when artificially juxtaposed, there is a wealth of physics at the interface between superconductors (*S*) and ferromagnets (*F*). Taking advantage of the competition between order parameters has lead to advances in the emerging field of superspintronics [1]. By placing an inhomogeneous magnetic texture at the *S*-*F* interface, it is possible to create the so-called long-ranged triplet component (LRTC) or finite-spin Cooper pair. Unlike the singlet Cooper pair, the LRTC is not dephased by the exchange field and can, therefore, penetrate further into a proximitized *F* layer. The manipulation of the LRTC opens the exciting possibility of performing spintronic logic operations on a dissipationless spin current [2]. Additionally, several breakthroughs in complex *S*-*F* heterostructures show promise as potential cryogenic memory elements. In such a scheme, information can be stored by the state of the system (superconducting or normal) [3,4] or the ground-state phase difference between two *S* layers in a *S*-*F*-*S* Josephson junction [5–9].

The prototypical superspintronic device is the superconducting spin valve. In this device, control of the magnetic state of the two *F* layers in a *S*-*F*-*F* or *F*-*S*-*F* heterostructure can be used to tune the generation of the LRTC [10–15]. The generation of the LRTC opens an additional conduction channel for Cooper pairs, resulting in the lowering of T_c [16]. In our previous work, we found this suppression of T_c to be of the order 10–20 mK in a 3*d* ferromagnet-niobium device [13], although other works have increased this effect to 130–140 mK by carefully engineering both the superconducting layer and *S*-*F* interface [12,15] and to over 1 K by both introducing a half-metal as the bottom *F* layer and changing the applied field orientation from an in-plane rotation to an in-plane to out-of-plane rotation [17,18]. The manipulation of the *F* layers in the superconducting spin valve requires careful engineering of the heterostructure and the rotation of the sample in an applied magnetic field. Under an in-plane field rotation, it is possible to introduce experimental artifacts due to vortex flow (if too high a current is applied, induced voltage from the vortex flow will dominate the transport signal), nonuniformity of field (if the sample is not aligned correctly, the out-of-plane field component will vary under rotation, modifying T_c), and temperature (a temperature gradient or local source of heating inside a cryostat is an important consideration when the sample is moving during measurement). Any of these can introduce a signal with the same periodicity as the signature of LRTC generation. A recent theoretical work considered that there exists a "half-select" problem in the multilayer spin-valve approach, which may be negated in a simplified device [19].

In this work, we describe a simplified *S*-*F* hybrid system, where the superconductivity can be controlled by a single adjacent *F* layer. The system requires only the ability to apply an external field in one direction (without the need for sample rotation), and we perform all our measurements in zero applied field, two distinct advantages over the superconducting spin valve. This control is achieved by coupling a superconducting Nb layer to rare-earth

*g.burnell@leeds.ac.uk

ferromagnetic Er, which has a large number of metastable magnetic phases accessible with the temperature or applied field. Previous work on holmium and dysprosium demonstrates the important role rare-earth ferromagnets will play in the implementation of superconducting spintronics in Josephson-type devices [20,21] and devices based on the control of T_c [22,23]. For example, Gu *et al.* [22] demonstrated that an antiferromagnetic to ferromagnetic transition in Ho resulted in modification of the T_c of an adjacent Nb layer of over 100 mK; however, the exact mechanism involved in the T_c shift was not established. This work was later expanded by producing trilayer samples of Ho/Nb/Ho and Dy/Nb/Dy in which a spin-valve-like effect of 400 mK was discovered [23]. These works established the ability to control T_c with the ferromagnetic texture in rare-earth ferromagnets; however, they lacked the theoretical description and the additional modification to the shape of the $R(T)$ transition reported in this manuscript.

Er is a trivalent rare-earth metal ($Z = 68$), with highly localized $4-f$ electrons and a hexagonal-close-packed (hcp) crystal structure. Competition between the Ruderman-Kittel-Kasuya-Yosida (RKKY) indirect exchange interaction and the crystalline anisotropy creates a rich magnetic phase diagram making this material ideal for the exploration of *S*-*F* proximity effects [24–31]. Below the high-temperature paramagnetic phase (approximately 85 K), Er first gains a sinusoidal, *c*-axis-modulated (CAM) antiferromagnetic phase. As the temperature is lowered, the magnetic wave vector of the CAM expands until approximately 52 K. Below this temperature, Er enters an "intermediate" phase where the in-plane moments begin to order creating what has been referred to by Cowley and Jensen [27] as an antiferromagnetic "wobbling cycloid." The magnetic cycloid repeat distance increases with decreasing temperature through a number of stable commensurate phases to eight atomic layers. These states exhibit a ferrimagnetic moment. Finally, below 18 K a conical *c*-axis ferromagnetic phase is formed. We are able to confirm that many of the magnetic states of bulk Er are reproducible in sputter-deposited epitaxial thin films and that these magnetic states can be controlled with either the temperature or applied magnetic field [32,33].

II. METHODS

The films are deposited using dc sputtering in a system with substrate heaters mounted above each sample slot. At the highest temperature, the base pressure of the system is approximately 10^{-7} mbar. This pressure improves as the system temperature is lowered. The samples are grown on 0.65-mm-thick *c*-plane Al_2O_3 substrates. The Nb is deposited at a nominal temperature of 700 °C, after which the system is cooled to 500 °C, a final thin Nb interface layer is deposited at this temperature, followed directly by the Er and then a 5-nm-thick Lu capping layer. Growth is performed at a typical Ar flow of 55 sccm resulting in Ar pressure of 2–3 μbar at a substrate-sample distance of 75 mm and at a typical growth rate of 0.1 nm s^{-1}. Growth rates are calibrated by fitting to Kiessig fringes obtained on single-layer samples by x-ray reflectometry. The Nb is grown first, as it is shown to be an effective buffer layer for the growth of rare-earth metals and stops the Er layer from reacting with oxygen in the substrate [34]. The Nb/Er interface is known to be sharp due to the lack of alloying and intermixing between the Nb and Er [35]. The Er grows epitaxially on the most densely packed Nb (110) plane in the Nishiyama-Wasserman orientation. The in-plane axis of hcp Er $[10\bar{1}0]$ is aligned with bcc Nb $[\bar{1}10]$ with 3:4 supercell commensuration in their nearest-neighbor distances along these axes [34]. Lu is chosen for the capping layer, as its lattice matches well with Er (preventing additional strain from being introduced), and unlike some traditional capping metals, such as Au, it can be deposited as a continuous layer at high temperatures [32].

Magnetization loops and remanent magnetization M_r are measured using a 6-T Quantum Design SQUID VSM magnetometer at 10 K. Electrical transport measurements are performed on sheet films using a conventional four-point-probe measurement configuration and employing two continuous-flow ^{4}He cryostats with maximum fields of 3 and 8 T. The field histories are applied only when the sample is in the normal state (to prevent flux trapping). The resistance as a function of the temperature $[R(T)]$ of the sample, from which T_c is obtained, is always measured at zero applied field. Temperature sweeps, both cooling and warming, are recorded to check for temperature hysteresis in the measurements. The temperature hysteresis (observable in Fig. 2) does not account for the observed T_c shift in Fig. 3.

III. RESULTS

A. Magnetic characterization

The magnetization vs field data along with minor loops for the Nb(20 nm)/Er(25 nm) bilayer sample at 10 K are shown as the inset in Fig. 1(a). The red squares show the initial magnetization and full magnetic hysteresis behavior for applied magnetic fields up to 60 kOe. The solid lines are a series of minor loops from which information about the M_r of the sample can be obtained. The M_r as a function of initial field data is collated in Fig. 1(a).

It is evident from Fig. 1(a) that for low initial fields, there is little change to the remanent state of the Er. This indicates that in this range, the stabilization of the spiral magnetic structure in the Er—due the RKKY interaction—is robust against perturbation by the externally applied magnetic fields. The large increase in M_r for initial fields of about 10 kOe is evidence that for initial field values greater than this, the Er does not reenter the same magnetic phase upon relaxation of the field. This is consistent with previous characterization work, which shows that at approximately 25 kOe there is a phase transition for an in-plane applied

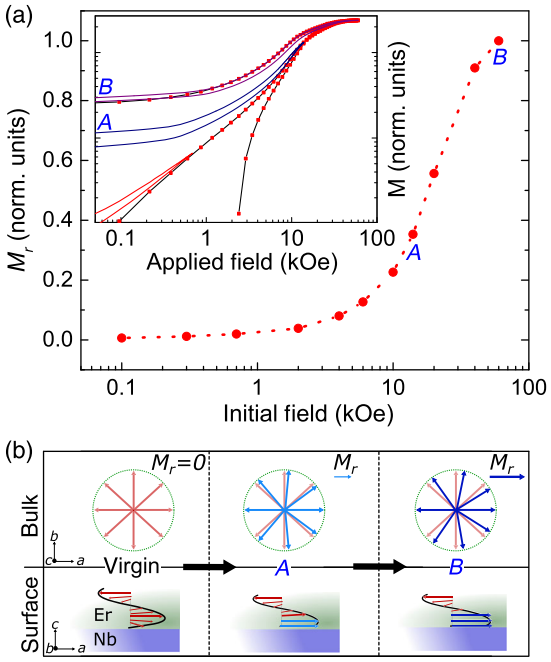

FIG. 1. (a) The normalized remanent magnetization M_r as a function of initial field. Inset: Positive quadrant of the magnetic hysteresis loop (squares) and exemplar minor loops (solid lines) of the bilayer at 10 K. The data are displayed on a log-log plot for increased clarity. (b) The two possible mechanisms to account for M_r. The bulk mechanism shows a canting of the spiral into the direction of the applied field. The surface mechanism shows an interface effect, where only the surface moments remain aligned in the direction of the applied field.

field into a distorted spiral phase known as the "fan" or "canted-fan" state [31,32]. The possible origins of the increased remanence are shown schematically in Fig. 1(b) and discussed further in Sec. IV A.

B. Electrical transport

Figure 2 shows the resistance as a function of the temperature for the Nb(20 nm)/Er(25 nm) bilayer sample, always measured in zero applied field. The data show the onset of superconductivity as the temperature is decreased for the virgin state (triangles) and after the application of an 80-kOe applied magnetic field (squares). In the inset of Fig. 2, the evolution of $R(T)$ as a function of the initial applied magnetic field can be seen. The resistance as a function of the temperature is always measured in zero applied magnetic field, and T_c is defined as 50% of the normal-state resistance. ΔT_c is calculated as the difference between T_c of the virgin state (triangles in Fig. 2) and T_c after the application and removal of a magnetic field. The ΔT_c data for all of the initial applied magnetic field values are collated in Fig. 3.

In Fig. 3, it is immediately clear that there is a strong link between the M_r of the Er and the T_c of the superconductor. This correlation between the properties of Er and Nb shows

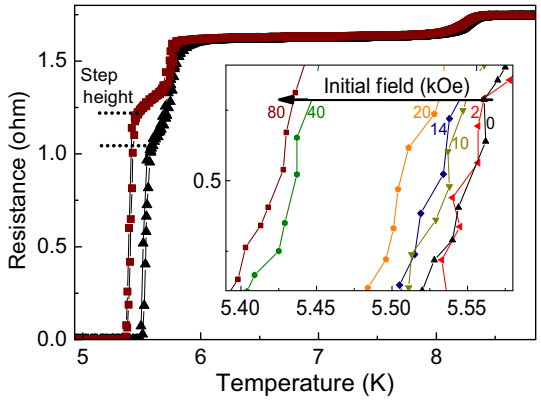

FIG. 2. Resistance as a function of temperature $[R(T)]$ for the virgin magnetic state (triangles) and post-80-kOe field saturation (squares). Both warming and cooling data are included, and the changing step heights are marked. Inset: Exemplar cooling curves demonstrating the evolution of $R(T)$ with initial field.

that both the T_c of the Nb and the magnetic state of the Er are strongly dependent on the field history of the sample. It also shows that there is a strong coupling between the superconducting and magnetic layers. The largest change to ΔT_c comes between 20 and 30 kOe, which, as we mention above, is also the field value where the Er state changes magnetic phase. After the application of the largest field possible in our system, 80 kOe, the T_c of the Nb is suppressed by approximately 140 mK, which is a large value reported for such a system. The metastable magnetic state obtained by applying and removing and initial field is robust against temperature changes in the measured range

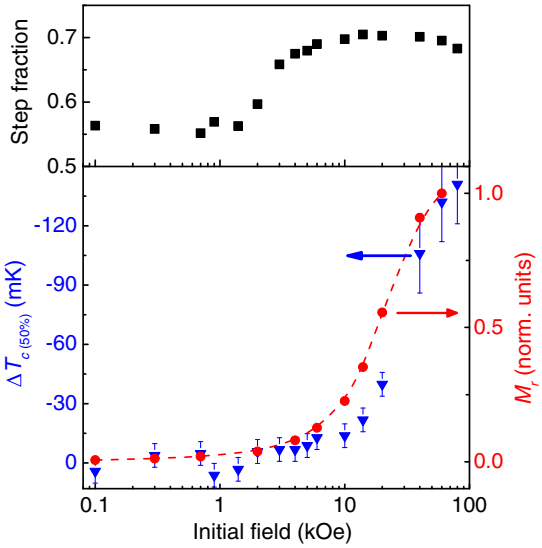

FIG. 3. Top panel: The fractional step height change with initial field. Bottom panel: The normalized remanent magnetization M_r (circles reproduced from Fig. 1) and the shift in superconducting critical temperature from the as-cooled state ΔT_c (triangles) as a function of initial applied magnetic field.

of 5–10 K. The system can be effectively reset to the virgin state by warming through the Curie temperature.

One additional point to note is the steplike features that are present in Fig. 2 and the fact that these steps also change with the field history. The height of the stepped feature in the transition is marked on Fig. 2. A step fraction is defined as the height of the step relative to the normal-state resistance (at 10 K). The collated step fraction is plotted in the upper panel of Fig. 3 and discussed further in Sec. V.

IV. MODELING

A. Modeling of M_r: An effective E_{ex}

Having established that the suppression observed in T_c is linked to the increased M_r, we now consider the local magnetic state of the Er film and propose two physical interpretations for the origin of M_r in Er. The first being a "bulk" modification of the spiral and the second a localized spin alignment at the Er surface.

As we have shown in our previous work, even in the thin film, Er has a highly complicated phase diagram [32,33]. Through a combination of temperature and field, the Er can be placed in a number of metastable magnetic states. For an in-plane field, between 20 and 30 kOe, Er undergoes a transition from the conical to a fan magnetic state canted into the direction of applied field. The subsequent removal of the applied field causes the Er to reenter the conical state; however, we argue the cone has now been modified and is canting in the direction of the external applied field, increasing M_r. This canted conical state is shown schematically as the top mechanism in Fig. 1(b).

It is well known that finite-size effects play an important part for thin-film rare-earths [36]. The long-range nature of the RKKY interaction (up to the sixth nearest neighbor) means that the reduced atomic coordination at the surfaces makes the spiral ends less robust against external perturbation, which clearly becomes more of an influencing factor for thinner films with a lower volume-to-surface-area ratio [33]. It is, therefore, possible that under the influence of an externally applied magnetic field, the spiral unwinds more readily at the surfaces and, being unable to overcome the energy barrier to reform the spiral, remains locally in the direction of the applied field. This is shown schematically as the bottom mechanism in Fig. 1(b). We calculate from the known thickness, saturation magnetization, and expected moment per atom that 0.65 nm (or just over two atoms) remaining aligned at the interface will account for the observed M_r (see the Supplemental Material [37] Fig. 1).

The bulk canted magnetic phase, which leads to a net magnetization, can be described by an effective exchange field if the coherence length inside the Er is (much) longer than the magnetic repeat unit of the helix, which is about 4 nm. On the other hand, the contribution of the surface moments to the total proximity effect is considerable only if the coherence length is short, comparable to the 0.65-nm effective Er thickness corresponding to aligned surface moments. The two mechanisms, thus, correspond to very different length scales of the coherence length inside the Er layer.

The resistance measurements of the Nb(20 nm)/Er(x nm) bilayers with Er layer thickness $x = 0$–25 nm suggest an approximate coherence length of 10 nm (see the Supplemental Material [37] Fig. 2), and in a related Ho system, the coherence length is estimated to be 30 nm [23]. This distance is far greater than 0.65 nm, and it is long enough to allow the Cooper pair to experience multiple helicies. It is, therefore, most likely that the Er undergoes the bulk transition to a new canted magnetic phase, which is retained at zero field, and that this is the origin of the suppression in T_c.

B. Modeling of ΔT_c vs M_r

To investigate the effect of an increased bulk remanent magnetization, we model it as an effective exchange field (J_z) in the F layer, which we can then link directly to the suppression in T_c.

Using the quasiclassical theory for superconductivity in the dirty limit (electronic mean free path much shorter than the phase coherence length), we calculate the critical temperature of an Er/Nb bilayer as a function of an effective exchange field inside the Er. We take the x axis normal to the metallic layers and assume translational invariance in the y-z plane. The Usadel equation for s-wave superconductivity then takes the form $i\hbar D\partial_x(\check{g}\partial_x\check{g}) = [\check{H}, \check{g}]$ with $\check{g}$ the 4×4 matrix Green function in the Nambu spin space, $\hbar$ the reduced Planck constant, and D the diffusion constant. For collinear exchange fields, the Hamiltonian can be described by $\check{H} = i\hbar\omega_n(\tau_3 \otimes \sigma_0) + \check{\Delta} - J_z\tau_0 \otimes \sigma_3$ (see, e.g., Ref. [38]) with J_z the exchange field directed along the z axis and ω_n the Matsubara frequencies defined by $\hbar\omega_n = \pi k_B T(2n + 1)$ with k_B the Boltzmann constant, n an integer, and the maximum allowed frequency given by the Debye frequency. x, y, z are defined such that J_z points along the direction of the net moment of the Er. Furthermore, σ_i and τ_i are the Pauli matrices of, respectively, the spin space and Nambu space. The matrix Green function and $\check{\Delta}$ have the following nonzero elements:

$$\check{g} = \begin{pmatrix} G_{\uparrow\uparrow} & 0 & 0 & F_{\uparrow\downarrow} \\ 0 & G_{\downarrow\downarrow} & F_{\downarrow\uparrow} & 0 \\ 0 & \bar{F}_{\uparrow\downarrow} & \bar{G}_{\uparrow\uparrow} & 0 \\ \bar{F}_{\downarrow\uparrow} & 0 & 0 & \bar{G}_{\downarrow\downarrow} \end{pmatrix},$$

$$\check{\Delta} = \begin{pmatrix} 0 & 0 & 0 & -\Delta \\ 0 & 0 & \Delta & 0 \\ 0 & -\Delta^* & 0 & 0 \\ \Delta^* & 0 & 0 & 0 \end{pmatrix}, \quad (1)$$

where G and F are the quasiclassical normal and anomalous Green functions respectively, both functions of (x, ω_n), and $\Delta(x)$ is the order parameter. The matrix Green function satisfies the normalization condition $\check{g}^2 = \check{1}$, and the order parameter must be solved selfconsistently satisfying the gap equation

$$i\Delta(\mathbf{R}) = \frac{\pi k_B T}{\ln(\frac{T}{T_{c0}}) + \sum_n (\frac{1}{|2n+1|})} \sum_{\omega_n} F_{\uparrow\downarrow}(\mathbf{R}, \omega_n) \quad (2)$$

with T_{c0} the bulk critical temperature. We use the interface boundary conditions as formulated by Nazarov [39], which for the interface between two materials with labels l, r for the layer on the left and right side of the interface, respectively, can be written as $\sigma_l \check{g}_l \partial_x \check{g}_l = \sigma_r \check{g}_r \partial_x \check{g}_r$ and $\sigma_l \check{g}_l \partial_x \check{g}_l = (2/R_b)[(\check{g}_l, \check{g}_r)/(4 + \Gamma(\check{g}_l \check{g}_r + \check{g}_r \check{g}_l - 2))]$, with σ_i the conductivity of layer i, $0 \leq \Gamma \leq 1$ the interface transparency, and R_b the interface resistance times the interface area $(\Omega\,\mathrm{m}^2)$.

The material parameters used for the Nb layer are $\xi_s = \sqrt{\hbar D_s/(2\pi k_B T_{c0})} = 7.9\,\mathrm{nm}$, $T_{c0} = 8.4\,\mathrm{K}$, and $\rho_s = 15.2\,\mu\Omega\mathrm{cm}$. Since the value of J_z is unknown, we explore various combinations of $\xi_f = \sqrt{\hbar D_f/J_z}$, J_z and R_b chosen such that the T_c of the bilayer corresponds to the experimental value of 5.5 K. The values of these parameters combined into sets are listed in the Supplemental Material [37] Table I. For all calculations, $\Gamma = 1$. For each material combination, T_c is calculated as a function of a shift in J_z (a shift of zero corresponding to the T_c of 5.5 K).

The results of the modeling are presented in Fig. 4 along with the experimental data. When taken with the Er thickness dependence (see the Supplemental Material [37] Fig. 2), it is parameter sets 2 and 5 which show closest agreement to the experimental data, although all parameter sets considered qualitatively reproduce the experimental data. These two parameter sets give the same value of interface resistance, but they are considered with different initial values of J_z, set 2 corresponding to the lowest temperature (approximately 22 K) conical ferromagnetic transition and set 5 the transition from the antiferromagnetic to ferromagnetic wobbling cycloid intermediate state (approximately 55 K), both of which are confirmed in our thin films [32]. From either starting point, the analysis shows that the observed 140-mK T_c shift corresponds to a (5–10)-K shift in J_z [$(7.5–15) \times 10^{-20}$ meV].

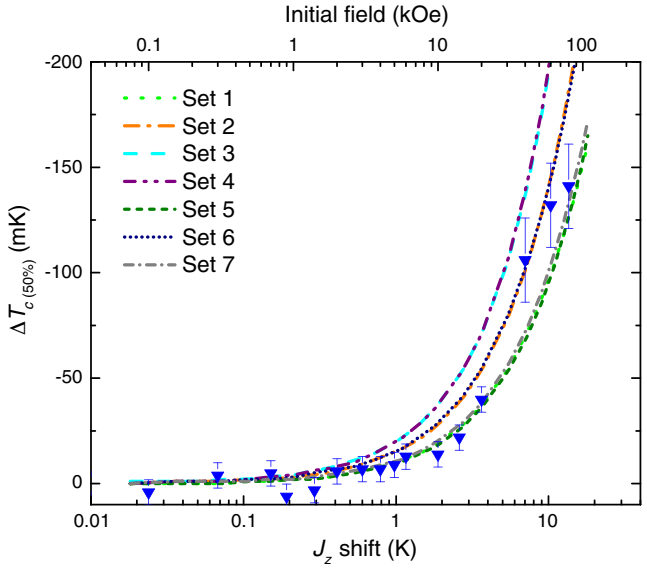

FIG. 4. The calculated suppression of T_c with an effective shift to the exchange field (J_z). Also plotted are the ΔT_c data from Fig. 3. The parameter "sets" used in the calculation are defined in the text and listed in the Supplemental Material [37] Table I.

V. DISCUSSION

Rare-earth ferromagnets, such as Er, offer a plethora of magnetic configurations in which a Cooper pair (coherent with a neighboring proximity coupled superconductor) can experience magnetic disorder. As a conical ferromagnet, Er is a theoretically ideal system in which to generate and study proximity effects induced by an additional LRTC [40]. In this work, it is expected that all $R(T)$ measurements are performed when the Er is in a disordered magnetic state. It is, therefore, not possible to directly attribute LRTC generation to the observed ΔT_c. In comparison to the superconducting spin valve, which has a clean LRTC on-off mechanism (as magnetic inhomogeneity is carefully engineered from otherwise homogeneous magnetic layers), our proposed origin of M_r cannot provide such a switching mechanism. The canting of the magnetic state into the direction of the applied field is unlikely to significantly change the conversion efficiency of singlet Cooper pairs into the LRTC. In the second proposed mechanism, spins at the surface remain aligned with the applied field and can create a homogeneous interface layer. From the spin-valve experimental argument, we expect this homogenous magnetic state to result in a decrease in LRTC generation and, therefore, an increase in T_c. This argument does not agree with the experimental observation in this work.

Given the size of this T_c effect is generally larger than that reported for spin valves (and the number of reported cases showing an effect opposite to the spin-valve effect, where the disordered magnetic state results in a *higher* measured T_c [22,41–43]), we urge caution for the interpretation of T_c measurements alone as evidence for the presence of the LRTC in S-F systems.

With the modeling, we show that the reported change in T_c can be described within the conventional S-F proximity theory by considering the increasing remanence of the Er as a shift in the effective exchange field. This increase in exchange field modifies the proximity effect, suppressing the T_c of the bilayer. An effective shift in J_z of 5–10 K accounts for the observed changes in T_c.

In the transition curves shown in Fig. 2, three steplike features can be seen. The first, present at approximately 8 K, appears to be directly related to the T_c of the bare Nb film. This is evidence of local regions of the bilayer film where the Er has no direct influence on the Nb, that is, where the two materials are not coupled by the proximity effect. One possibility for decoupling is at the Er grain boundaries or local regions around the wire-bond contacts, where the force of the contact may have disrupted the Nb/Er interface. This interpretation is supported by the observation that there is no significant field history dependence of this step.

Some common explanations for steplike features in the transition curves can be ruled out for our system. The sputtering technique employed in this work is unlikely to create a significant thickness gradient. To check the uniformity of the films, a (20×20)-mm^2 film is diced into several pieces and x-ray reflectivity is performed. A 5% variation in thickness is observed, and this variation is only slightly greater than the error in individually calculated thickness by fitting to Kiessig fringes. By comparison, the sample size for transport measurements is only (3×3) mm^2, where uniformity in film thickness will be very high. Crystallographic inhomogeneity is a further possibility, but again unlikely. We examine a possible current (heating) dependence of the steplike features using currents ranging from 100 nA up to 1 mA, but we find no such evidence and current-induced local heating can, thus, be ruled out. There are no known Nb/Er alloys, and in our previous reflectivity work, we observed no evidence for intermixing at the interface [33], which, if possible, can alter the superconducting properties of the Nb. Poor interface transparency can cause anomalous features in resistivity around the superconducting transition, as current paths change to flow preferentially through the superconductor. The formation of an oxide barrier at the interface causes such effects, but the calculated oxidation time in our vacuum of 15 min is far longer than the 20 s between the final Nb and Er layer depositions. The steps are never observed in either single-layer Nb films (deposited under identical growth conditions) or films of Nb grown in proximity to a homogeneous ferromagnet such as Co (see, for example, Ref. [13]).

Steplike features have been observed previously in works coupling BCS superconductors to inhomogeneous ferromagnetic textures. For example, Witt [44] and Chiodi *et al.* [45] in helical Ho/Nb bilayers, Zhu *et al.* [46] in GdN/Nb/GdN spin valves [46], and Zhu *et al.* [42] in striped domain $(\mathrm{Co/Pt})_n$/Nb multilayers where it appears that the step shape can be modified by defining a current path parallel (no inhomogeneity, no step) or perpendicular (inhomogeneity, step) to the stripe domains.

While the exact origin of the step is unknown, it appears linked to the *S*-*F* proximity effect in all examples above. In this work, we observe in the upper panel of Fig. 3 that the height of the step as a fraction of the transition is field history dependent. This step-height change occurs at a different field than the largest changes in M_r and ΔT_c. While the change in step height does not appear to be intrinsically linked to the change in T_c, it is still clearly linked to the magnetic state of the Er layer. This further supports that the origin of the step is a fundamental feature of the *S*-*F* proximity effect requiring theoretical description.

VI. CONCLUSIONS

In summary, the remanent state of Er when proximity coupled to a Nb superconductor can have a strong influence on T_c. The application of magnetic field is able to change the metastable magnetic state of the Er from a conical to a fan state. This modification results in a fundamental change to the shape and temperature of the superconducting transition to zero resistivity.

We hope the observation of this unconventional effect proves fruitful for refinement of *S*-*F* theory, particularly with the lack of current description of the stepped transition observed in this (and many similar) systems.

A shift in T_c of 140 mK is much larger than previously observed for singlet domain-wall effects and is comparable to the largest observed by the generation of the LRTC in the context of the superconducting spin valve with 3*d* ferromagnets. This system fulfills the requirements for cryogenic memory based upon the proposed architecture of Oh *et al.* [3], and we offer this materials system as a candidate for future superspintronic device application.

The data associated with this paper are openly available from the University of Leeds data repository [47].

ACKNOWLEDGMENTS

The authors thank the UK Engineering and Physical Sciences Research Council (EPSRC) (Grants No. EP/J010634/1, No. EP/J010650/1, No. EP/I031014/1, and No. EP/J01060X/1) for their financial support. N. S. acknowledges JEOL Europe and ISIS neutron and muon source for Ph.D. funding.

[1] J. Linder and J. W. A. Robinson, Superconducting spintronics, Nat. Phys. **11**, 307 (2015).
[2] M. Eschrig, Spin-polarized supercurrents for spintronics, Phys. Today **64**, No. 1, 43 (2011).
[3] S. Oh, D. Youm, and M. R. Beasley, A superconductive magnetoresistive memory element using controlled exchange interaction, Appl. Phys. Lett. **71**, 2376 (1997).
[4] A. Potenza and C. H. Marrows, Superconductor-ferromagnet CuNi/Nb/CuNi trilayers as superconducting spin-valve core structures, Phys. Rev. B **71**, 180503 (2005).
[5] C. Bell, G. Burnell, C. W. Leung, E. J. Tarte, D.-J. Kang, and M. G. Blamire, Controllable Josephson current through a pseudospin-valve structure, Appl. Phys. Lett. **84**, 1153 (2004).

[6] E. Goldobin, H. Sickinger, M. Weides, N. Ruppelt, H. Kohlstedt, R. Kleiner, and D. Koelle, Memory cell based on a φ Josephson junction, Appl. Phys. Lett. **102**, 242602 (2013).

[7] B. Baek, W. H. Rippard, S. P. Benz, S. E. Russek, and P. D. Dresselhaus, Hybrid superconducting-magnetic memory device using competing order parameters, Nat. Commun. **5**, 3888 (2014).

[8] B. M. Niedzielski, S. G. Diesch, E. C. Gingrich, Y. Wang, R. Loloee, W. P. Pratt, and N. O. Birge, Use of Pd-Fe and Ni-Fe-Nb as soft magnetic layers in ferromagnetic Josephson junctions for nonvolatile cryogenic memory, IEEE Trans. Appl. Supercond. **24**, 1 (2014).

[9] E. C. Gingrich, B. M. Niedzielski, J. A. Glick, Y. Wang, D. L. Miller, R. Loloee, W. P. Pratt, and N. O. Birge, Controllable 0-π Josephson junctions containing a ferromagnetic spin valve, Nat. Phys. **12**, 564 (2016).

[10] P. V. Leksin, N. N. Garif'yanov, I. A. Garifullin, Ya. V. Fominov, J. Schumann, Y. Krupskaya, V. Kataev, O. G. Schmidt, and B. Büchner, Evidence for Triplet Superconductivity in a Superconductor-Ferromagnet Spin Valve, Phys. Rev. Lett. **109**, 057005 (2012).

[11] A. A. Jara, C. Safranski, I. N. Krivorotov, C.-T. Wu, A. N. Malmi-Kakkada, O. T. Valls, and K. Halterman, Angular dependence of superconductivity in superconductor/spin-valve heterostructures, Phys. Rev. B **89**, 184502 (2014).

[12] X. L. Wang, A. Di Bernardo, N. Banerjee, A. Wells, F. S. Bergeret, M. G. Blamire, and J. W. A. Robinson, Giant triplet proximity effect in superconducting pseudo spin valves with engineered anisotropy, Phys. Rev. B **89**, 140508 (2014).

[13] M. G. Flokstra, T. C. Cunningham, J. Kim, N. Satchell, G. Burnell, P. J. Curran, S. J. Bending, C. J. Kinane, J. F. K. Cooper, S. Langridge, A. Isidori, N. Pugach, M. Eschrig, and S. L. Lee, Controlled suppression of superconductivity by the generation of polarized Cooper pairs in spin-valve structures, Phys. Rev. B **91**, 060501 (2015).

[14] M. G. Flokstra, N. Satchell, J. Kim, G. Burnell, P. J. Curran, S. J. Bending, J. F. K. Cooper, C. J. Kinane, S. Langridge, A. Isidori, N. Pugach, M. Eschrig, H. Luetkens, A. Suter, T. Prokscha, and S. L. Lee, Remotely induced magnetism in a normal metal using a superconducting spin-valve, Nat. Phys. **12**, 57 (2016).

[15] P. V. Leksin, N. N. Garif'yanov, A. A. Kamashev, A. A. Validov, Ya. V. Fominov, J. Schumann, V. Kataev, J. Thomas, B. Büchner, and I. A. Garifullin, Isolation of proximity-induced triplet pairing channel in a superconductor/ferromagnet spin valve, Phys. Rev. B **93**, 100502 (2016).

[16] Ya. V. Fominov, A. A. Golubov, T. Yu Karminskaya, M. Yu Kupriyanov, R. G. Deminov, and L. R. Tagirov, Superconducting triplet spin valve, JETP Lett. **91**, 308 (2010).

[17] A. Singh, S. Voltan, K. Lahabi, and J. Aarts, Colossal Proximity Effect in a Superconducting Triplet Spin Valve Based on the Half-Metallic Ferromagnet CrO_2, Phys. Rev. X **5**, 021019 (2015).

[18] S. Voltan, A. Singh, and J. Aarts, Triplet generation and upper critical field in superconducting spin valves based on CrO_2, Phys. Rev. B **94**, 054503 (2016).

[19] N. G. Pugach, M. Safonchik, T. Champel, M. E. Zhitomirsky, E. Lähderanta, M. Eschrig, and C. Lacroix, Superconducting spin valves controlled by spiral re-orientation in MnSi, arXiv:1702.08828.

[20] I. Sosnin, H. Cho, V. T. Petrashov, and A. F. Volkov, Superconducting Phase Coherent Electron Transport in Proximity Conical Ferromagnets, Phys. Rev. Lett. **96**, 157002 (2006).

[21] J. W. A. Robinson, J. D. S. Witt, and M. G. Blamire, Controlled injection of spin-triplet supercurrents into a strong ferromagnet, Science **329**, 59 (2010).

[22] Y. Gu, J. W. A. Robinson, M. Bianchetti, N. A. Stelmashenko, D. Astill, F. M. Grosche, J. L. MacManus-Driscoll, and M. G. Blamire, Magnetic state controllable critical temperature in epitaxial Ho/Nb bilayers, APL Mater. **2**, 046103 (2014).

[23] Y. Gu, G. B. Halász, J. W. A. Robinson, and M. G. Blamire, Large Superconducting Spin Valve Effect and Ultrasmall Exchange Splitting in Epitaxial Rare-Earth-Niobium Trilayers, Phys. Rev. Lett. **115**, 067201 (2015).

[24] M. Habenschuss, C. Stassis, S. K. Sinha, H. W. Deckman, and F. H. Spedding, Neutron diffraction study of the magnetic structure of erbium, Phys. Rev. B **10**, 1020 (1974).

[25] D. Gibbs, J. Bohr, J. D. Axe, D. E. Moncton, and K. L. D'Amico, Magnetic structure of erbium, Phys. Rev. B **34**, 8182 (1986).

[26] H. Lin, M. F. Collins, T. M. Holden, and W. Wei, Magnetic structure of erbium, Phys. Rev. B **45**, 12873 (1992).

[27] R. A. Cowley and J. Jensen, Magnetic structures and interactions in erbium, J. Phys. Condens. Matter **4**, 9673 (1992).

[28] D. A. Jehan, D. F. McMorrow, J. A. Simpson, R. A. Cowley, P. P. Swaddling, and K. N. Clausen, Collapsing cycloidal structures in the magnetic phase diagram of erbium, Phys. Rev. B **50**, 3085 (1994).

[29] B. Watson and N. Ali, Magnetic transitions in single-crystal erbium, J. Phys. Condens. Matter **7**, 4713 (1995).

[30] B. Watson and N. Ali, The *b*-axis magnetic phase diagram of erbium, J. Phys. Condens. Matter **8**, 1797 (1996).

[31] B. H. Frazer, J. R. Gebhardt, and N. Ali, Magnetic phase diagrams of erbium, J. Appl. Phys. **85**, 6100 (1999).

[32] J. D. S. Witt, J. F. K. Cooper, N. Satchell, C. J. Kinane, P. J. Curran, S. J. Bending, S. Langridge, L. J. Heyderman, and G. Burnell, Magnetic phases of sputter deposited thin-film erbium, Sci. Rep. **6**, 39021 (2016).

[33] N. Satchell, J. D. S. Witt, G. Burnell, P. J. Curran, C. J. Kinane, T. R. Charlton, S. Langridge, and J. F. K. Cooper, Probing the spiral magnetic phase in 6 nm textured erbium using polarised neutron reflectometry, J. Phys. Condens. Matter **29**, 055801 (2017).

[34] J. Kwo, M. Hong, and S. Nakahara, Growth of rare-earth single crystals by molecular beam epitaxy: The epitaxial relationship between HCP rare earth and BCC niobium, Appl. Phys. Lett. **49**, 319 (1986).

[35] W. G. Moffatt, *The Handbook of Binary Phase Diagrams* (General Electric Company, Schenectady, NY, 1981), Vol. 4.

[36] J. Bohr, D. Gibbs, J. D. Axe, D. E. Moncton, K. L. d'Amico, C. F. Majkrzak, J. Kwo, M. Hong, C. L. Chien, and J. Jensen, Diffraction studies of rare earth metals and superlattices, Physica (Amsterdam) **159B**, 93 (1989).

[37] See the Supplemental Material at http://link.aps.org/supplemental/10.1103/PhysRevApplied.7.044031 for a list of parameters used in the theoretical modeling of the system

and further data on the dependence of T_c with Er thickness and applied field (both in and out of plane).

[38] T. Löfwander, T. Champel, J. Durst, and M. Eschrig, Interplay of Magnetic and Superconducting Proximity Effects in Ferromagnet-Superconductor-Ferromagnet Trilayers, Phys. Rev. Lett. **95**, 187003 (2005).

[39] Y. V. Nazarov, Novel circuit theory of Andreev reflection, Superlattices Microstruct. **25**, 1221 (1999).

[40] D. Fritsch and J. F. Annett, Proximity effect in superconductor/conical magnet/ferromagnet heterostructures, New J. Phys. **16**, 055005 (2014).

[41] A. Yu. Rusanov, M. Hesselberth, J. Aarts, and A. I. Buzdin, Enhancement of the Superconducting Transition Temperature in Nb/Permalloy Bilayers by Controlling the Domain State of the Ferromagnet, Phys. Rev. Lett. **93**, 057002 (2004).

[42] L. Y. Zhu, T. Y. Chen, and C. L. Chien, Altering the Superconductor Transition Temperature by Domain-Wall Arrangements in Hybrid Ferromagnet-Superconductor Structures, Phys. Rev. Lett. **101**, 017004 (2008).

[43] L. Y. Zhu, Yaohua Liu, F. S. Bergeret, J. E. Pearson, S. G. E. te Velthuis, S. D. Bader, and J. S. Jiang, Unanticipated Proximity Behavior in Ferromagnet-Superconductor Heterostructures with Controlled Magnetic Noncollinearity, Phys. Rev. Lett. **110**, 177001 (2013).

[44] J. D. S. Witt, Ph.D. thesis, University of Cambridge, 2012.

[45] F. Chiodi, J. D. S. Witt, R. G. J. Smits, L. Qu, G. B. Halász, C.-T. Wu, O. T. Valls, K. Halterman, J. W. A. Robinson, and M. G. Blamire, Supra-oscillatory critical temperature dependence of Nb-Ho bilayers, Europhys. Lett. **101**, 37002 (2013).

[46] Y. Zhu, A. Pal, M. G. Blamire, and Z. H. Barber, Superconducting exchange coupling between ferromagnets, Nat. Mater. **16**, 195 (2016).

[47] https://doi.org/10.5518/142.